RESEARCH ARTICLE

Bone regeneration in Ds-Red pig calvarial defect using allogenic transplantation of EGFP-pMSCs – A comparison of host cells and seeding cells in the scaffold

Ming-Kai Hsieh[1,2,3,4], Chia-Jung Wu[2,3], Xuan-Chun Su[5], Yi-Chen Chen[1,5,6], Tsung-Ting Tsai[2,3,4], Chi-Chien Niu[2,3,4], Po-Liang Lai[2,3,4]*, Shinn-Chih Wu[1,5,6]*

1 Institute of Biotechnology, National Taiwan University, Taipei, Taiwan, 2 Department of Orthopaedic Surgery, Chang Gung Memorial Hospital, Taoyuan, Taiwan, 3 Bone and Joint Research Center, Chang Gung Memorial Hospital, Taoyuan, Taiwan, 4 College of Medicine, Chang Gung University, Taoyuan, Taiwan, 5 Department of Animal Science and Technology, National Taiwan University, Taipei, Taiwan, 6 Center for Biotechnology, National Taiwan University, Taipei, Taiwan

* polianglai@gmail.com (PLL); scw01@ntu.edu.tw (SCW)

Abstract

Background

Cells, scaffolds, and factors are the triad of regenerative engineering; however, it is difficult to distinguish whether cells in the regenerative construct are from the seeded cells or host cells via the host blood supply. We performed a novel *in vivo* study to transplant enhanced green fluorescent pig mesenchymal stem cells (EGFP-pMSCs) into calvarial defect of DsRed pigs. The cell distribution and proportion were distinguished by the different fluorescent colors through the whole regenerative period.

Method/Results

Eight adult domestic Ds-Red pigs were treated with five modalities: empty defects without scaffold (group 1); defects filled only with scaffold (group 2); defects filled with osteoinduction medium-loaded scaffold (group 3); defects filled with 5×10^3 cells/scaffold (group 4); and defects filled with 5×10^4 cells/scaffold (group 5). The *in vitro* cell distribution, morphology, osteogenic differentiation, and fluorescence images of groups 4 and 5 were analyzed. Two animals were sacrificed at 1, 2, 3, and 4 weeks after transplantation. The *in vivo* fluorescence imaging and quantification data showed that EGFP-pMSCs were represented in the scaffolds in groups 4 and 5 throughout the whole regenerative period. A higher seeded cell density resulted in more sustained seeded cells in bone regeneration compared to a lower seeded cell density. Host cells were recruited by seeded cells if enough space was available in the scaffold. Host cells in groups 1 to 3 did not change from the 1st week to 4th week, which indicates that the scaffold without seeded cells cannot recruit host cells even when enough space is available for cell ingrowth. The histological and immunohistochemical data showed that more cells were involved in osteogenesis in scaffolds with seeded cells.

Conclusion

Our *in vivo* results showed that more seeded cells recruit more host cells and that both cell types participate in osteogenesis. These results suggest that scaffolds without seeded cells may not be effective in bone transplantation.

Introduction

Skeletal defects require surgery using bone grafts. Autografts are the gold standard for bone grafting [1]; however, donor site morbidity and the limited amount of available donor tissue restrict their application [2, 3]. Regenerative tissue engineering using cells, scaffolds, factors and blood supply [4] has become an alternative method to treat skeletal bone defects.

Allografts may provide the same osteoconductive conduit for bony fusion as traditional autografts and may have comparable biomechanical properties without amount restriction [5, 6]. Although depleted of osteoprogenitor cells like mesenchymal stem cells (MSCs), the fusion rate still reaches 73% to 100% in instrumented spinal fusion [7–16], making allograft a clinically feasible alternative form of fusion. The role of cells in allograft prompted us to wonder if seeded cells are necessary in bone regeneration clinically.

MSCs are undifferentiated multipotent cells with the capacity to differentiate into osteoblasts, chondrocytes, adipocytes, fibroblasts, and other tissues of mesenchymal origin [17]. MSCs lack expression of costimulatory molecules like CD40, CD80, and CD86, which makes them largely non-immunogenic [18], as supported by evaluations of their immunosuppressive properties using mitogen proliferation assays [19]. Due to these suitable transplantation properties, MSCs are an important material in developmental biology and transgenic methods, as well as in potential clinical applications in tissue engineering and gene therapy [20, 21].

Some studies have found that seeded MSCs may be capable of releasing major growth factors, reducing the immune response, mobilizing the host's cells or eventually directly differentiating into osteoblasts [22–25]. The expansion, proliferation, migration, viability and osteogenic differentiation of MSCs on different types of scaffolds have been shown in studies [26–31], but the role of seeded MSCs is still poorly addressed. Histologically, it is difficult for us to distinguish cells in the regenerative construct from seeded MSCs or from host MSCs via the host blood supply. In this study, we transplanted EGFP pig MSCs into calvarial defect of DsRed pigs. The cell distribution and proportion were distinguished by different fluorescent colors throughout the whole regenerative period.

The purpose of the present study was to clarify the distribution and proportion of seeded cells and host cells by tracking two fluorescent cells in the same scaffold in a pig critical-sized calvarial defect model.

Materials and methods

EGFP-pMSCs culture in the scaffold

Scaffold. A hemostatic gelatin sponge, Spongostan (Ferrosan Medical Device, MS0003, thickness 0.1 cm), was used as the 3D scaffold [32]. Scanning electron microscopy (SEM) (Hitachi, SU8220) analysis indicated a mean pore size of approximately 148 ± 62 μm (Fig 1). To perform transplantation, the scaffolds were cut into disks with a diameter of 0.8 cm, sterilized by 75% (v/v) ethanol and washed three times with phosphate-buffered saline. The sterile scaffold disks were then immersed in Opti-MEM medium (Gibco) before use.
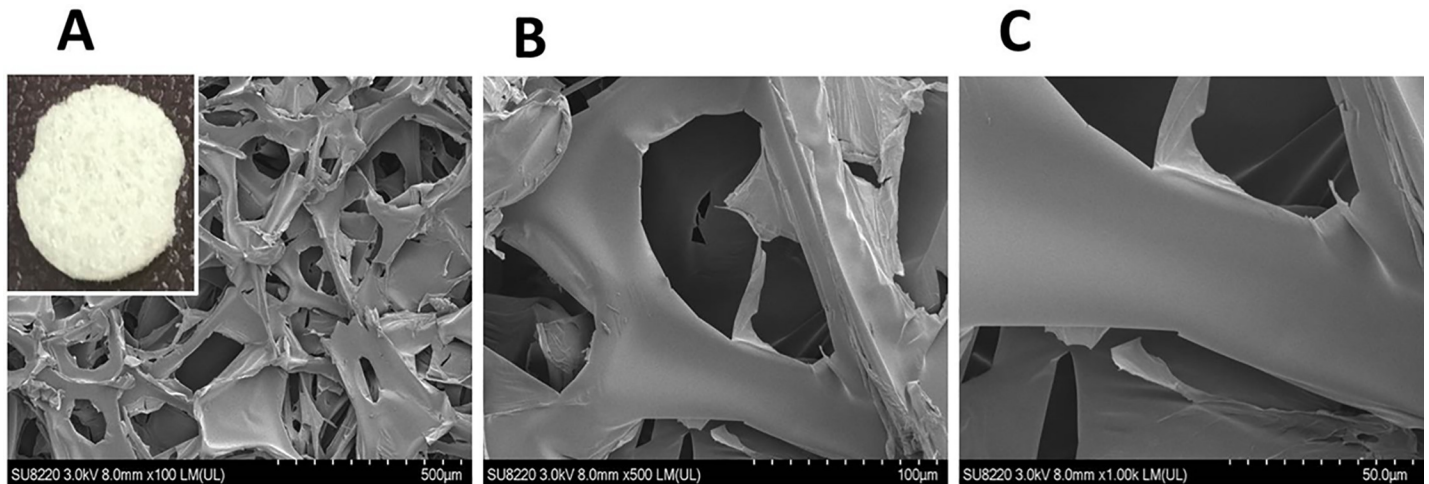
Fig 1. Morphology of the scaffold. The Hemostatic Gelatin Sponge, Spongostan (Ferrosan Medical Device, MS0003, Thickness 0.1 cm) was used as the 3D Scaffold and determined by SEM (Scanning Electron Microscopy) to have a mean pore size of approximately 148 ± 62 µm. Increased magnification was observed from A to C.

Cell culture. The EGFP-pMSCs were isolated and cultured from bone marrow aspirate which obtained from transgenic pigs harboring an EGFP gene. Passage 5 EGFP-pMSCs [19] were cultured in minimum essential medium alpha (MEM-α) (Gibco) supplemented with 10% fetal bovine serum (HyClone) and antibiotic solutions (100 U/mL penicillin, 100 µg/mL streptomycin, 50 µg/mL gentamicin and 250 ng/mL fungizone) (Gibco). The cells were maintained in a humidified 37°C incubator supplied with 5% CO_2.

Seeding of cells. The sterile scaffold disks were individually placed onto the wells of a 48 well-plate. The cell seeding density was 5×10^3 or 5×10^4 cells/disk. Cells in 50 µL of medium were seeded throughout the surface of the scaffold disk and incubated for 3 hours to allow cell attachment before the addition of medium. The culture condition was observed by fluorescent microscopy and recorded until the 28th day after seeding onto scaffolds.

In vitro cell distribution and morphology analysis

The cell scaffold constructs were washed twice with phosphate buffered saline (PBS; GIBCO, Invitrogen Corp., Carlsbad, CA) and fixed in 1.5% v/v glutaraldehyde in 0.14M sodium cacodylate (pH 7.4) for 30 mins at room temperature. Dehydration was performed by sequential immersion in serial diluted ethanol solutions of 50, 60, 70, 80, 90, and 100% v/v. The samples were then transferred to hexamethyldisilazane and air-dried at room temperature overnight. The cell distribution and morphology were analyzed by SEM and confocal laser scanning microscopy (CLSM) (Bio-Rad MRC 600).

In vitro osteogenic differentiation

The above two groups then received 0.5 mL/well of osteogenic induction medium (OIM) to promote cell differentiation. The OIM medium was composed of complete MEM-α medium enriched with 10^{-7} M dexamethasone (Sigma), 10 mM β- glycerophosphate (Sigma) and 50 µg/mL ascorbic acid (Sigma) [32]. The OIM medium was replenished every two or three days for a total of 7 days. The osteogenic potential was assessed using an alkaline phosphatase staining and Alizarin red S (ARS) staining.

Alkaline phosphatase staining and quantification

The osteogenic potential was assessed using an ALP assay kit (BioVision K412-500) after 7 days. The cells were washed twice with ice-cold PBS and lysed using 300 μL of RIPA (radioimmunoprecipitation assay) lysis buffer (Sigma-Aldrich Corp., St Louis, MO, USA) for 5 mins on ice. The cells were then rapidly scraped from the plate, and the cell lysates/RIPA buffer were transferred to a 1.5-mL microcentrifuge tube on ice for 20 min, followed by centrifugation at 8000 g for 10 min at 4˚C. The supernatant was then added to a new 1.5-mL microcentrifuge tube and stored at -20˚C. 50 μL of 5 mM pNPP solution was added to each well containing the test samples and the aliquots were incubated for 60 min at 25˚C while protected from light. Subsequently, 20 μL of the stop solution was added to terminate the ALP activity in the sample. The absorbance at 405 nm was measured with a spectrophotometer (UV-Vis 8500). Then, the ALP activity was calculated using the following formula: ((optical density–mean optical density of the control wells) × total volume × dilution)/(18.45 × sample volume).

Alizarin red S (ARS) staining and quantification

Cells cultured on the discs at different time points were washed twice with PBS and fixed with 4% paraformaldehyde for 15 min. The fixative was removed, and the discs with cells were rinsed with deionized water. The scaffolds were stained with a 2% ARS staining kit (ScienCell) for 5 mins to clarify the calcium deposits. The staining solution was discarded, and the scaffolds were carefully washed with deionized water to remove excess stain. The staining results were captured with a digital camera. To quantify the staining of each scaffold, 1 mL/disc of 10 wt% cetylpyridinium chloride (Sigma) was added to the discs. The discs were left on an orbital shaker (speed, 60 rpm) for 1 h to completely resolve the dye from the discs. Finally, 100 μL of the dissolved solution from each scaffold was placed into a well of a 96-well plate, and the absorbance was measured at 540 nm with an ELISA reader.

In vivo experimental design

Eight adult domestic Ds-Red pigs (average age of 15 ± 3months) with a mean weight of 100 ±20 kgs were obtained from the Department of Animal Science, National Taiwan University (Taipei, Taiwan). This study was carried out in strict accordance with the recommendations in the *Guide for the Care and Use of Laboratory Animals* of the National Institutes of Health. All animals were used under approved animal protocols by the Institutional Animal Care and Use Committee of National Taiwan University (NTU107-EL-00128) and housed accordingly.

The five treatment modalities were empty defects without scaffold (group 1; n = 1); defects filled with only scaffold (group 2; n = 1); defects filled with osteoinduction medium-loaded scaffold (group 3; n = 1); defects filled with 5×10^3 cells/scaffold (group 4; n = 2) and defects filled with 5×10^4 cells/scaffold (group 5; n = 2).

Seven defects were created in each animal. The treatment modalities of the defects were determined for each animal separately by a randomization chart.

Operation

Zoletil (5 mg/kg body weight) was injected in the neck area of the pig intramuscularly as a sedative. All experimental procedures were performed under a standard anesthetic/ analgesic protocol as described in previous studies [19, 33].

The frontal bone was exposed after a standard sagittal approach in the forehead region. Identical bony defects were then created with a saline-cooled trephine burr (diameter 8 mm, depth 2 mm) meeting the requirements for a critical size defect in pigs [34]. The defects were
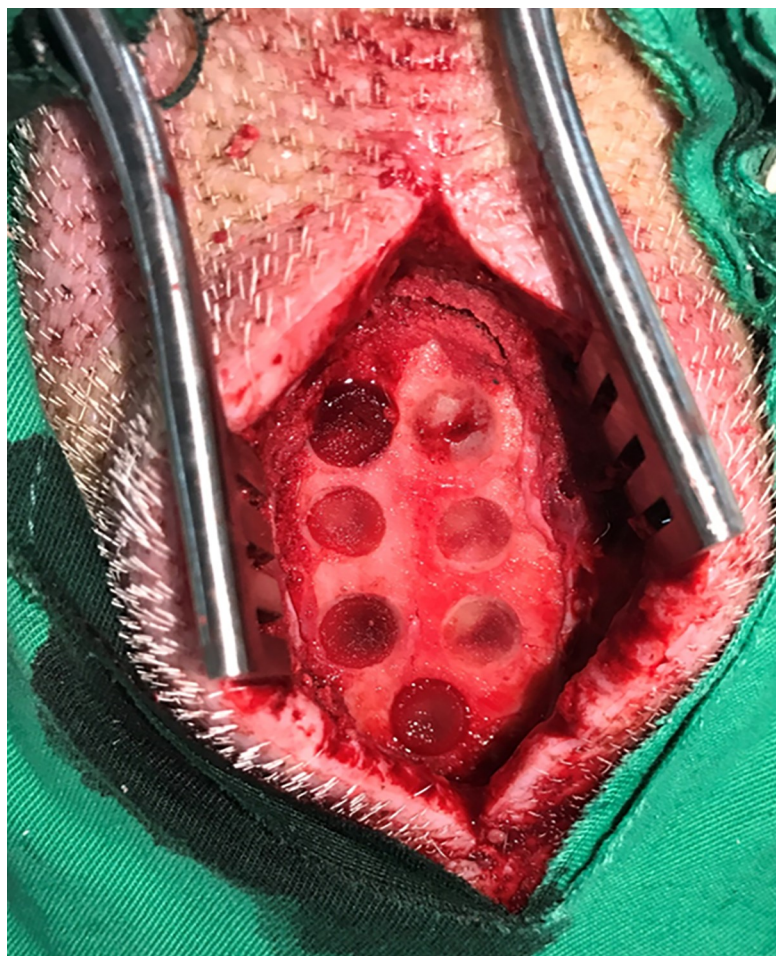
Fig 2. Critical-sized calvarial defects of DsRed pig were created. The frontal bone was exposed after a standard sagittal approach in the forehead region. Seven identical bony defects were created in the frontal bone and the defects were positioned at least 5mm apart to minimize biological interactions. The internal plate of the neurocranium remained completely intact during the procedure. After adequate hemostasis, the scaffolds were implanted.

https://doi.org/10.1371/journal.pone.0215499.g002

positioned at least 5 mm apart to minimize biological interactions [35]. The internal plate of the neurocranium remained completely intact during the procedure. After well hemostasis, the scaffold was implanted (Fig 2). The periosteum and skin over the defects were sutured in two layers with resorbable material (Vicryl USP 3–0; Vicryl USP1-0; Ethicon Johnson & Johnson, NJ, USA).

Sacrifice and preparation of specimens

Two animals were sacrificed 1, 2, 3, and 4 weeks after transplantation. The animals were anesthetized by intramuscular injection of tiletamine-zolazepam and atropine and then were euthanized with a lethal injection of sodium pentobarbital. The frontal bone was en bloc resected, and the calvarial defects were retrieved separately using an oscillating autopsy saw. The retrieved specimens were fixed in 10% neutral formalin for further survey.

In vivo fluorescence imaging

All samples were washed twice with PBS, fixed in 4% v/v formaldehyde (methanol-free; Polyscience) for 15 min, permeabilized with 0.1% v/v Triton X-100 for 5 min, and incubated in 10

mg/mL bovine serum albumin and 100 g/mL RNase for 45 min at room temperature. F-actin filaments were stained with Alexa Fluor-conjugated phalloidin (Molecular Probes) for 20 min, and nuclei were counterstained with 10 g/mL propidium iodide (Sigma) for 10 min. Finally, the samples were washed with PBS and mounted in Vectashield. CLSM images were acquired on a BioRad MRC 600 microscope. The quantitative distribution of the two types of fluorescent cells was analyzed by using NIH Image J software (National Institutes of Health, USA) and presented as the modified integrated density (Modified IntDen). The modified integrated density was calculated based on the selected Integrated Density—(Area of selected cell ×Mean fluorescence of background readings).

Histology

The tissue samples were processed to obtain non-decalcified ground sections. After 2 weeks in 10% neutral formalin, the specimens were rinsed in running tap water, trimmed, dehydrated in ascending concentrations of ethanol, and embedded in methyl methacrylate. The embedded tissue blocks were serially cut into 5-μm-thick ground sections using a microtome (Leica SM 2000; Germany) and mounted on glass slides. Ten cross-sections from the middle of each implant were stained with hematoxylin-eosin and Masson's trichrome and visualized using an optical microscope (DXM200F Digital Camera; Nikon, Tokyo, Japan).

Immunohistochemistry of CD68

After fixation in formalin, the dissected blocks were decalcified for 11 days in 10% EDTA and subsequently embedded in paraffin. In brief, after removal of the embedding material, endogenous peroxidases were blocked with H_2O_2. Semi-thin sections were rinsed in saline and incubated in phosphate-buffered citrate solution, pH 7.4 (Sigma-Aldrich Corp., St Louis, MO, USA), for 20 min in the microwave and rinsed with phosphate-buffered saline. A microtome was used to obtain 3-mm-thick sections. Immunohistochemistry analysis of tissue labelled with anti-CD68 was performed with purified ab81289 (Abcam Inc., Cambridge, MA) at 1:250. Heat-mediated antigen retrieval was performed using Tris/EDTA buffer pH 9.0 (Abcam Inc., Cambridge, MA). Goat Anti-Rabbit IgG H&L (HRP) was used as the secondary antibody at 1/500. The negative control used PBS instead of the primary antibody, and counterstaining was performed with hematoxylin. The qualitative analysis was performed using a light microscope (Nikon Eclipse E600).

Immunohistochemistry of osteogenic related markers

Histological slides were incubated with citrate buffer (Dako, Glostrup, Denmark) at 60˚C for heat-induced epitope retrieval and blocked with 1% hydrogen peroxide/methanol (Sigma-Aldrich, St Louis, MO, USA) for 30 min at room temperature. Subsequently, they were incubated overnight at 4˚C with primary antibodies osteocalcin (1:1000, sc-365797, Santa Cruz Biotechnology, CA,USA), Bone Sialoprotein II (BSP-II) (1:100,sc-73630, Santa Cruz Biotechnology, CA,USA), and collagen type I (Col-I) (1:1000, sc-59772, Santa Cruz Biotechnology, CA,USA).The color reaction was developed with ready-to-use 3,3'-diaminobenzidine (Dako Liquid DAB) color solution.The slides were counterstained with hematoxylin and visualized by a light microscope (Nikon Eclipse E600, Tokyo, Japan). The negative control used PBS instead of the primary antibody, and counterstaining was performed with hematoxylin.

Statistical analysis

All experimental results are expressed as the mean ± SD, and the statistical analysis was performed using Student's t-test and two-way ANOVA. Analysis of variance (ANOVA) was performed by using Statistica 6.0 software (Statsoft, Tulsa, OK, USA). Differences with a p value of < 0.05 were considered statistically significant.

Results

In vitro characterization of EGFP-pMSCs

Passage 5 EGFP-pMSCs [20] were collected by incubation with 0.25% trypsin-EDTA for 5 min at 37°C and re-suspended in ice-cold washing buffer consisting of PBS with 2% FBS. Phase-contrast images of EGFP-MSCs showed a change from a round-shaped to a spindle-shaped morphology after culture for 1 day. After 2 days of culture, 90% confluence was reached, and the cells were trypsinized and re-plated at a dilution of 1:3. These EGFP-pMSCs proliferated rapidly and harbored a greater abundance of EGFP expression by fluorescence microscopy (Fig 3).

In vitro fluorescence evaluation

The sterile scaffolds were individually placed onto the wells of a 48 well-plate. The cell seeding density was 5×10^3 or 5×10^4 cells/scaffold in 50 μL of medium, and the cells were seeded
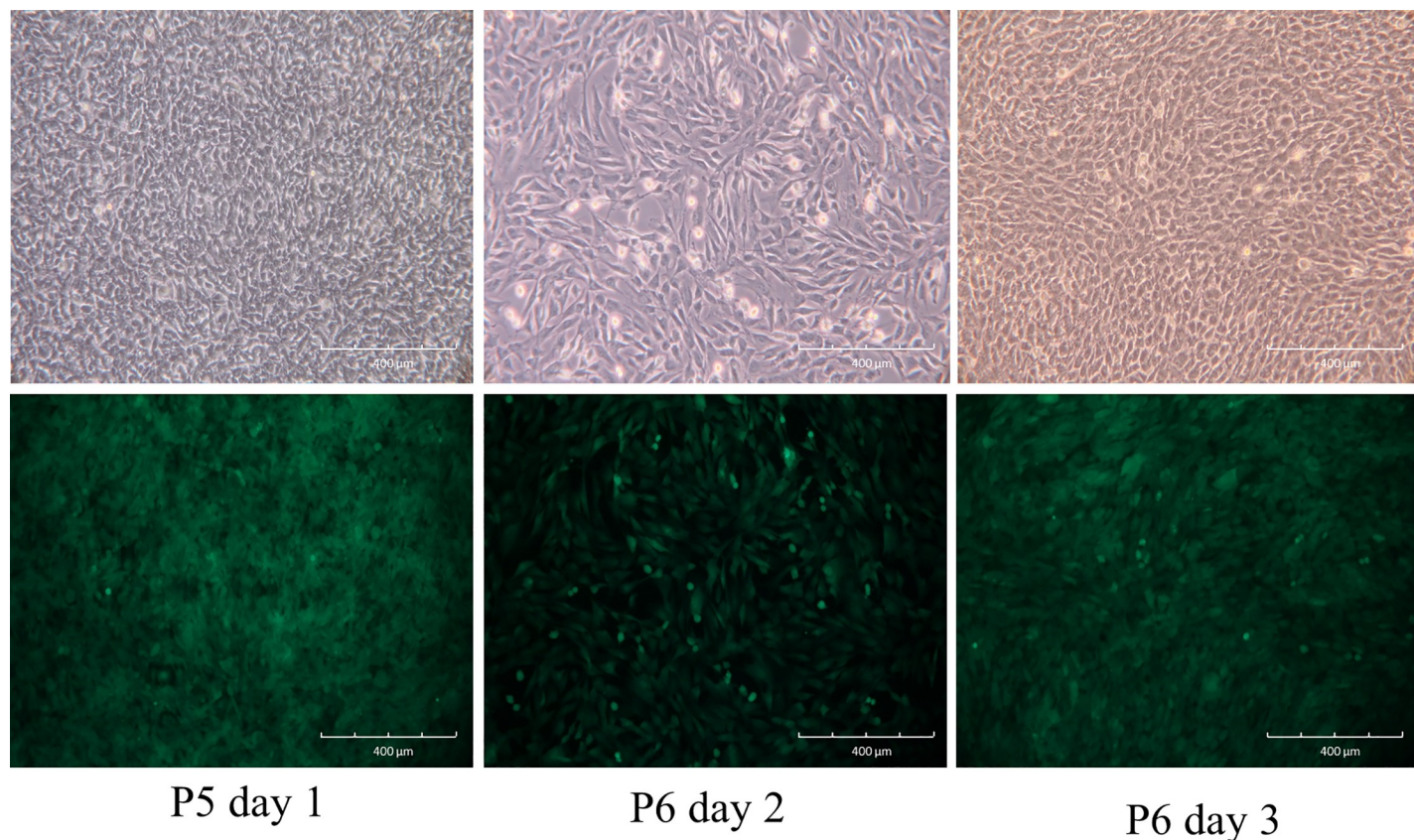

P5 day 1   P6 day 2   P6 day 3

Fig 3. Cell culture of EGFP-MSCs. Phase-contrast image of passage 5 EGFP-MSCs showing the change from round-shaped to spindle-shaped morphology after culture for 1 day (Upper Row). After 2 days of culture, 90% confluence was reached, and the cells were trypsinized and re-plated at a dilution of 1:3. These EGFP-pMSCs proliferated rapidly and harbored a greater abundance of EGFP expression according to fluorescence microscopy (lower row).
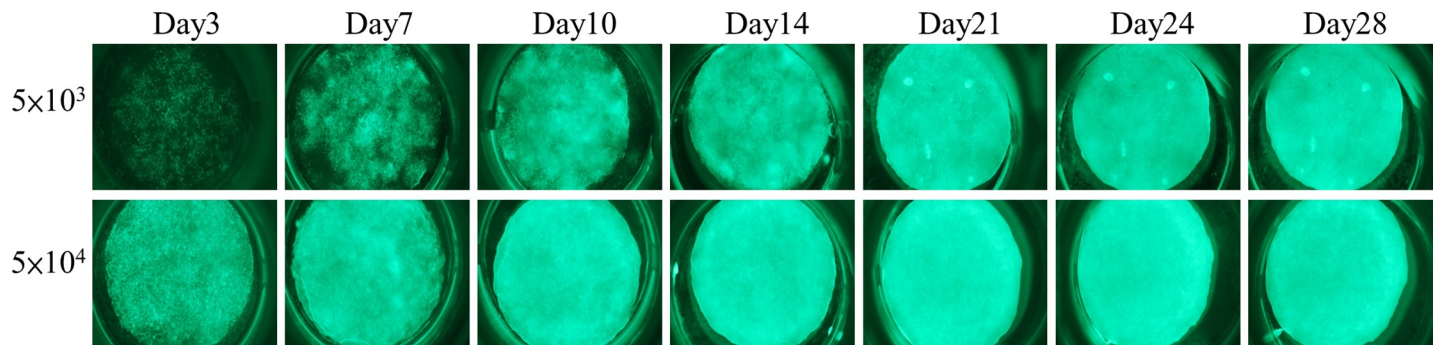
https://doi.org/10.1371/journal.pone.0215499.g003

Fig 4. *In vitro* fluorescence evaluation of two different loading density in the scaffolds. An increase in the expression of green fluorescence was observed from day 3 to day 28 in both groups by fluorescence microscopy, especially in the 5 x 10^4 group.

throughout the top side of the scaffold and then incubated for 3 h to allow cell attachment before adding the maintenance medium. From day 3, osteoinduction medium was added, and increasing expression of green fluorescence from day 3 to day 28 was observed in both groups by fluorescent microscopy, especially in the 5 x 10^4 group (Fig 4).

In vitro cell distribution and morphology analysis

SEM analysis showed that this biodegradable and biocompatible scaffold [36] with a mean pore size of approximately 148 ± 62 μm was suitable for growth of the EGFP-pMSCs. The intensity of live cells increased from day 3 to 28, indicating sufficient intricate space available for ingrowth. SEM images indicated that the EGFP-pMSCs spread on the sponge, and cellular extension and networks were observed. The connected pores were nearly covered by cells by day 21 in the 5×10^4 group and by day 28 in the 5×10^3 group (Fig 5). CLSM images of the *in vitro* distribution of EGFP-pMSCs in the scaffolds were obtained from day 3 to day 28 (Fig 6). The constructs were washed with PBS and mounted in Vectashield. CLSM images were acquired on a BioRad MRC 600 microscope (100X). Three-dimensional z-stack images were
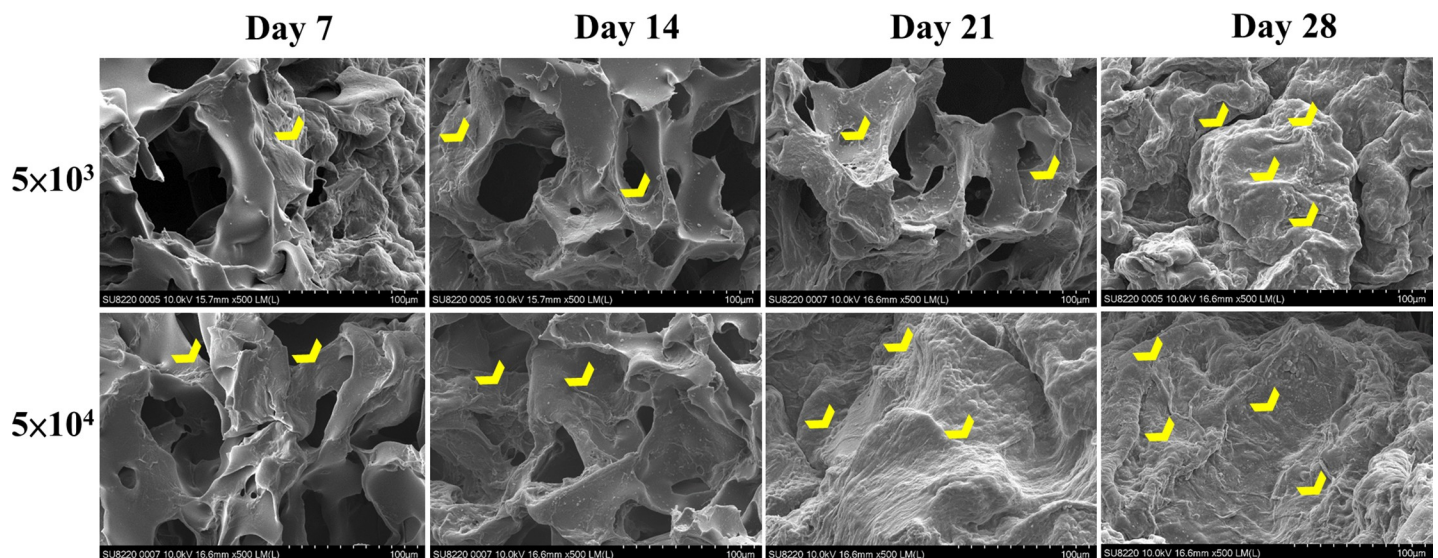

Fig 5. *In vitro* SEM analysis. SEM images indicated that the EGFP-pMSCs (yellow heads) spread on the sponge, and cellular extension and networks between them were observed from day 7 to day 28 in both groups. The connected pore was nearly covered by cells at day 21 in the 5×10^4 group and day 28 in the 5×10^3 group.
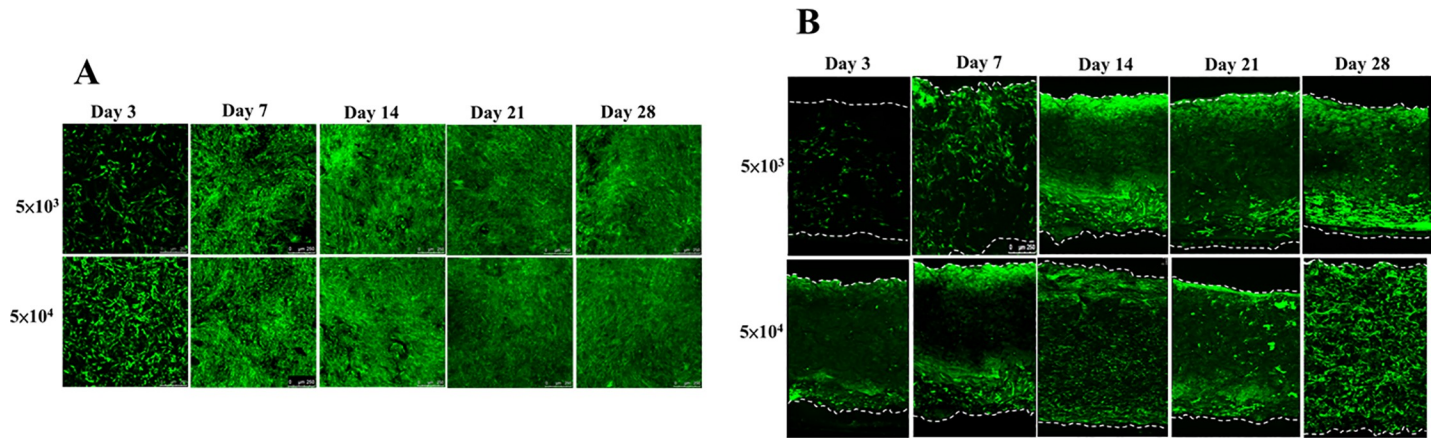
Fig 6. CLSM images of the *in vitro* distribution of EGFP-pMSCs in the scaffolds. The green fluorescence distribution in both groups corresponded to the cell density, especially in the surface view (A). In the cross section of the scaffold (B), cells were distributed into the scaffold from the surface to the center from day 3 to day 28.

evaluated and merged. The distribution of green fluorescence in both groups corresponded to the cell density, especially in the surface view (Fig 6A). In the cross section of the scaffold (Fig 6B), cells were distributed into the scaffold from the surface to the center from day 3 to day 28. On day 28, more cells were observed in the central area in the 5×10^4 group than the 5×10^3 group, and the space seemed to be sufficient for cell growth in both groups.

In vitro osteogenic differentiation

Alkaline phosphatase staining and quantification. The alkaline phosphatase staining results on the culture plates were observed by microscopy (Fig 7A). Both groups showed slight positive staining on day 7, and the relative staining intensity increased on days 14, 21, and 28 compared to days 0 and 7 in the 5×10^3 cell group. In the 5×10^4 cell group, the staining intensity increased significantly from day 7. In both groups, the staining intensity continued to slowly increase steadily from day 21 to day 28. Alkaline phosphatase is an early marker of bone formation, and the level increased significantly in the first 2 weeks, followed by a slow steady increase until day 28. Alkaline phosphatase activity (Fig 7B) showed that the cells seeded in the two groups were able to produce alkaline phosphatase on days 7, 14, 21, and 28, and the enzyme activity was significantly higher in the 5×10^4 group than the 5×10^3 group between days 7 and 28 ($^{**} p < 0.01$, $^{***} p < 0.001$), indicating higher osteoblast differentiation in the 5×10^4 group.

Alizarin red S (ARS) staining and quantification. Alizarin red S staining (Fig 8A) is indicative of bone mineralization and was negative on day 7 in both groups. Up to day 14, all groups showed positive staining with a deep red color, indicating bone nodule formation. The alizarin red staining quantification assay (Fig 8B) was performed at different time points, and the absorbance was measured at 540 nm using an ELISA reader. The absorbance value significantly increased from day 7 to days 14, 21 and 28. The values were significantly higher in the 5×10^4 group than in the 5×10^3 group on day 14 and 21 ($p<0.05$), consistent with the results of alkaline phosphatase staining.

In vivo fluorescence imaging

Confocal laser scanning microscopy was performed to image groups 1 through 5 from week 1 to week 4. (Fig 9). EGFP-pMSCs were present in the scaffolds in groups 4 and 5 through the
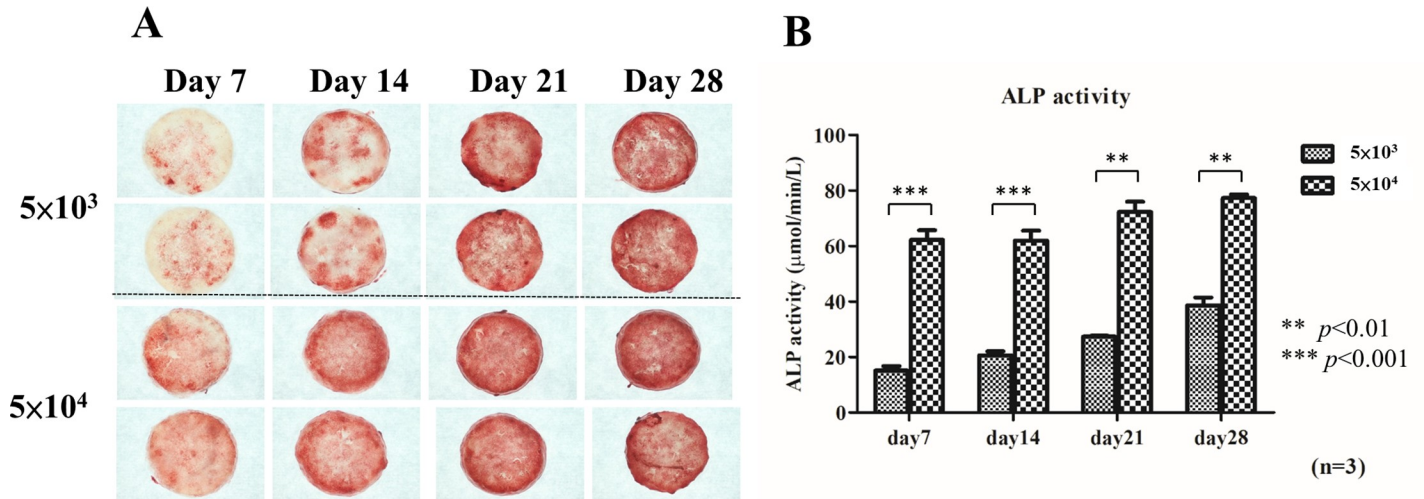
Fig 7. Alkaline phosphatase staining and quantification analysis. Microscopy observation of alkaline phosphatase staining results on the culture plates (A). Both groups showed slight positive staining on day 7, and the relative staining intensity increased on days 14, 21, and 28 compared to Days 0 and 7 in the 5×10^3 cell group. In the 5×10^4 cell group, the staining intensity increased significantly from day 7. Alkaline phosphatase activity (B) showed the enzyme activity was significantly higher in the 5×10^4 group than the 5×10^3 group from days 7 to 28 (** $p < 0.01$, *** $p < 0.001$), indicating higher osteoblast differentiation in the 5×10^4 group. Data is shown as mean ± standard deviation.

whole period. Although the EGFP expression decreased in the third and fourth weeks, DsRed expression increased in groups 4 and 5. The green fluorescence was higher in group 5 than in group 4 at each time point, similar to the *in vitro* fluorescence imaging results (Fig 6A).

DsRed expression was significantly higher in groups 2 and 3 than in group 1 at each time point, which indicated that the empty scaffold facilitates DsRed cells ingrowth. Even at week 4, no sufficient two fluorescent cells were observed in group 1, which indicates that this type of
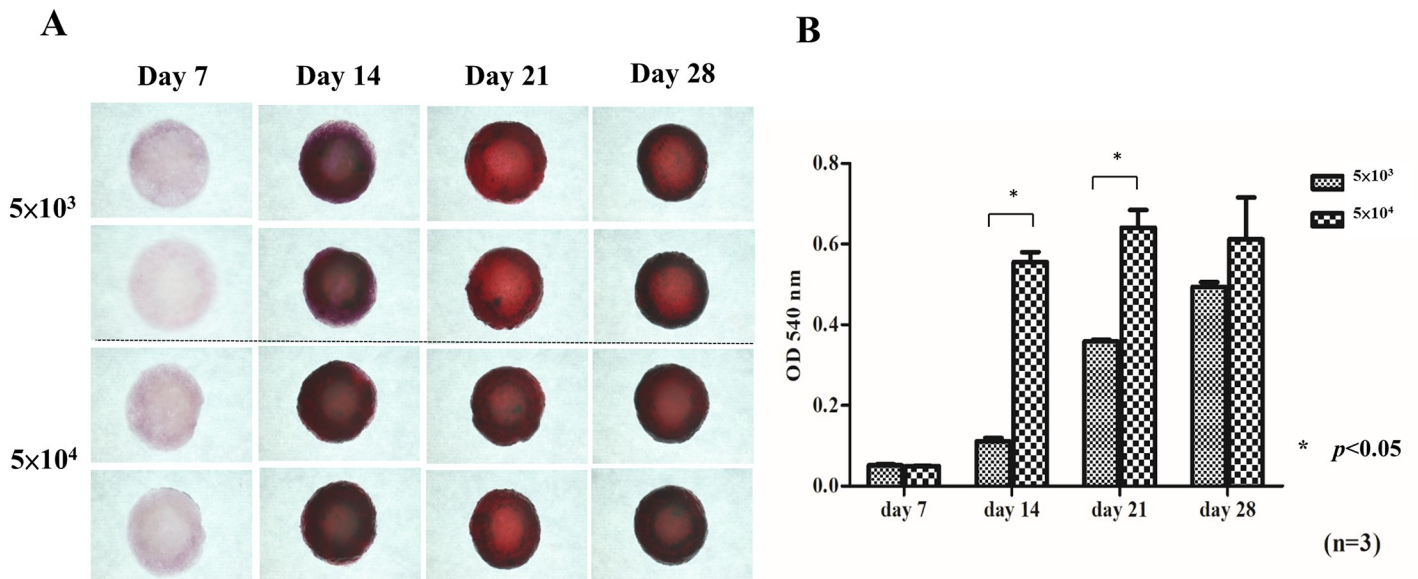

Fig 8. Alizarin red S staining and quantification analysis. Alizarin red S staining (A) was negative on day 7 in both Groups. Up to day 14, all groups showed positive staining with deep red color, indicating bone nodule formation. Alizarin red staining quantification assays (B) were performed at different time points. The absorbance value increased significantly from day 7 to days 14, 21 and 28. The values were significantly higher in the 5×10^4 group than in the 5×10^3 group on day 14 and 21. Differences considered significant at * $p < 0.05$ were marked. Data is shown as mean ± standard deviation.
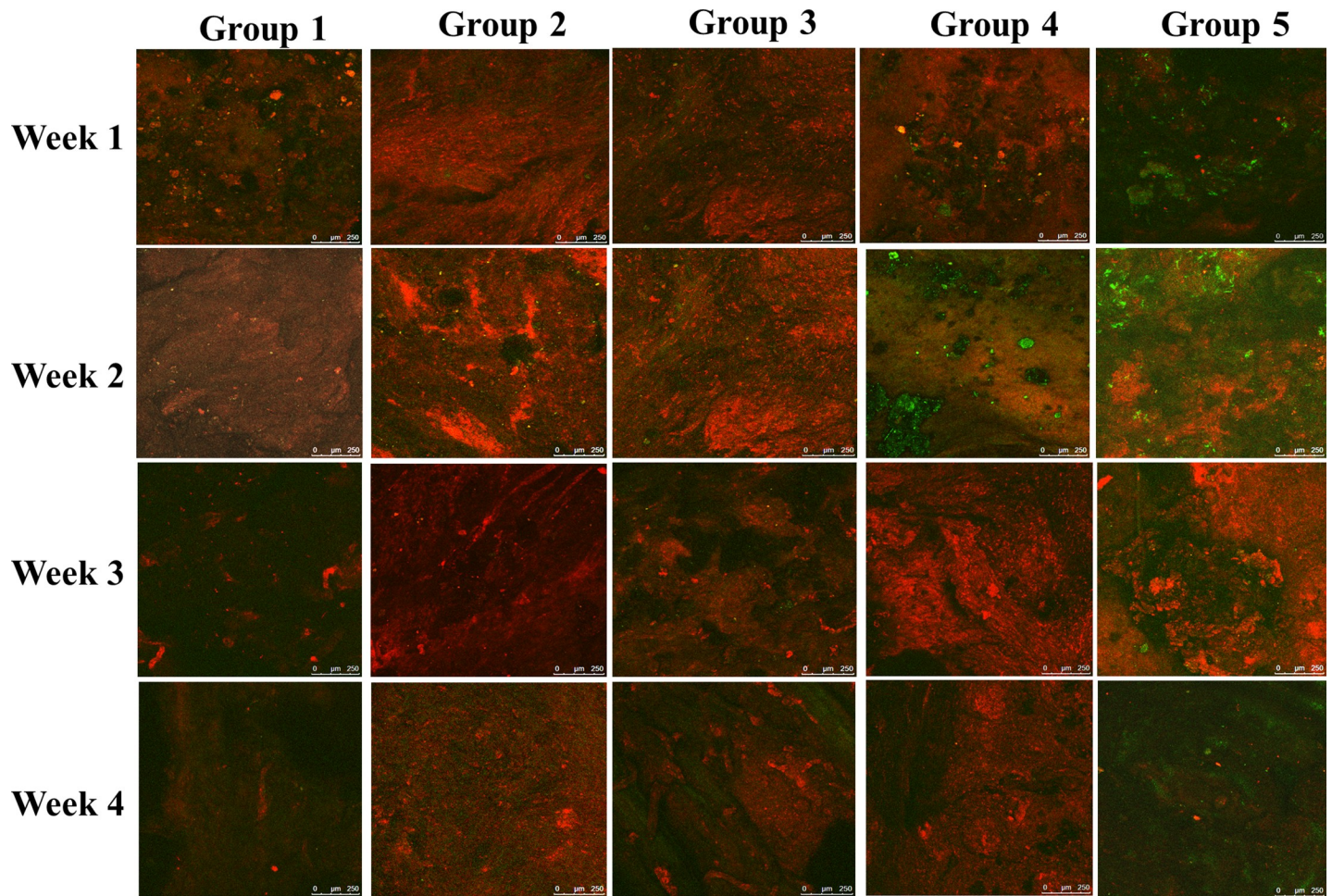
Fig 9. CLSM image of group 1 to 5 from week 1 to week 4. EGFP-pMSCs were present in the scaffolds in groups 4 and 5 from week 1 to week 4. Although EGFP expression decreased in the third and fourth weeks, DsRed expression was increased in groups 4 and 5. Green fluorescence was higher in group 5 than in group 4 at each time point, similar to the *in vitro* fluorescence distribution result. DsRed expression was significantly higher in groups 2 and 3 than in group 1 at each time point, which indicated that the empty scaffold facilitates DsRed cells ingrowth. Even at week 4, no sufficient two fluorescent cells were observed in group 1.

calvarial defect cannot heal spontaneously during the bone healing period used in our experiments.

In vivo fluorescence quantification

The modified integrated density of green and DsRed fluorescence in the acquired images was measured using Image J and expressed as bar graphs (Fig 10). EGFP expression (Fig 10A) was higher in Groups 4 and 5 than in the other three groups from the 1st week to the 3rd week ($p < 0.05$; $p < 0.01$) and was significantly highest in group 5 in the 4th week ($p < 0.05$). These results indicate that the seeded cells were present in the scaffold and that the higher load of seeded cells was sustained until the 4th week. The results of the *in vivo* study were compatible with those of the *in vitro* study. By the 4th week, EGFP expression in Group 4 decreased to the levels in Groups 1–3, which means that an insufficient number of seeded cells may not be effective for tissue transplantation. EGFP expression was highest in the 2nd week, which means that the proliferation of seeded cells reached its highest peak, consistent with the *in vitro* ALP/ARS staining results (Figs 7 and 8).
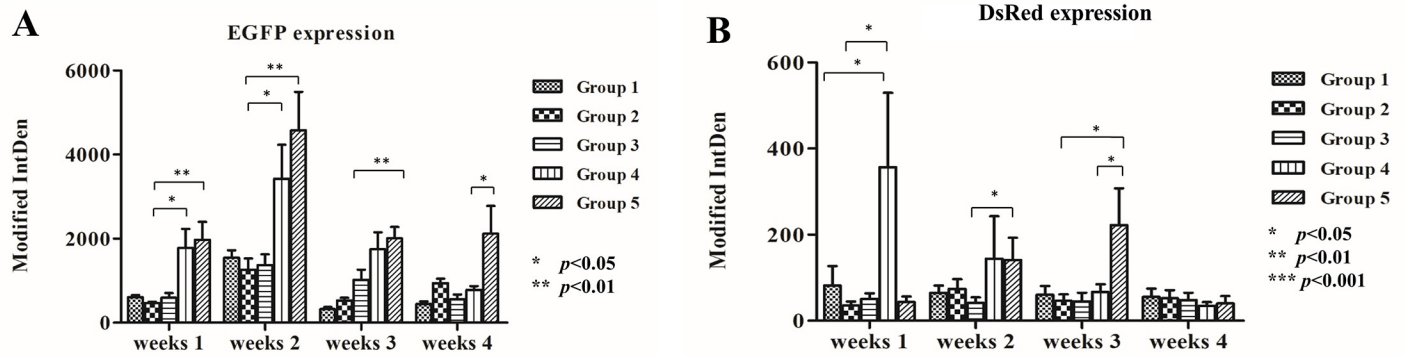
Fig 10. *In vivo* fluorescence quantification. EGFP (A) and DsRed (B) expression using Modified IntDen in Group 1 to 5 from week 1 to 4 were demonstrated as bar chart. Differences considered significant at * $p < 0.05$, ** $p < 0.01$, and *** $p < 0.001$ respect to control. Data is shown as mean ± standard deviation.

In the 1st week, DsRed expression (Fig 10B) was higher in Group 4 than in the other groups, indicating that recruitment of host cells was facilitated by the scaffold seeded with a lower density of cells compared with the empty scaffold or scaffold seeded with a higher density of cells. DsRed expression decreased from the 1st week to 4th week in group 4 but increased in group 5, which means that more EGFP pMSCs can recruit more host cells 2 weeks after transplantation and that enough available space and higher cell loading can benefit tissue regeneration. The DsRed expression in groups 1 to 3 did not increase from the 1st week to 4th week, indicating that the empty scaffold attracted host cells only in the first week after transplantation and implying that scaffolds without seeded cells may not be effective for tissue transplantation. Osteogenic differentiation may be responsible for the decreased expression of EGFP and DsRed expression from week 2 to week 4 in groups 4 and 5.

Histological analysis

Hematoxylin and eosin staining and Masson's trichrome staining were analyzed using a light microscope at various levels of magnification.

A greater number of cells were stained with H&E in groups 4 and 5 compared to groups 1–3 in the first week (Fig 11). In the fourth week, obvious deposition of osteoids (yellow arrowhead) was noted in group 5. Calcification of the osteoids led to the formation of primitive trabecular bone in group 5 compared with group 4 in the fourth week. In Groups 1–3, cells were sustained until the fourth week, but no obvious osteoids were found in the 4th week.

Masson's trichrome staining of cells increased in all groups in week 1 through 4, but blue-colored osteoid-like tissue was only found in groups 4 and 5 after the third week (Fig 12). In the 4th week, connective fibrous tissue with a large amount of undifferentiated cells was noted in groups 1, 2, and 3 (yellow arrowhead). Meanwhile, in groups 4 and 5, thick dense fibrous connective tissue with differentiated osteoblast-like cells (yellow arrow) was noted.

Immunohistochemistry of CD68

The levels of the macrophage marker [37] CD68 were higher in groups 4 and 5 than in the other groups in the fourth week (Fig 13), especially around the neovascularization area. The increase in macrophages indicated an increase in osteoclasts and, consequently, more osteogenesis in groups 4 and 5.
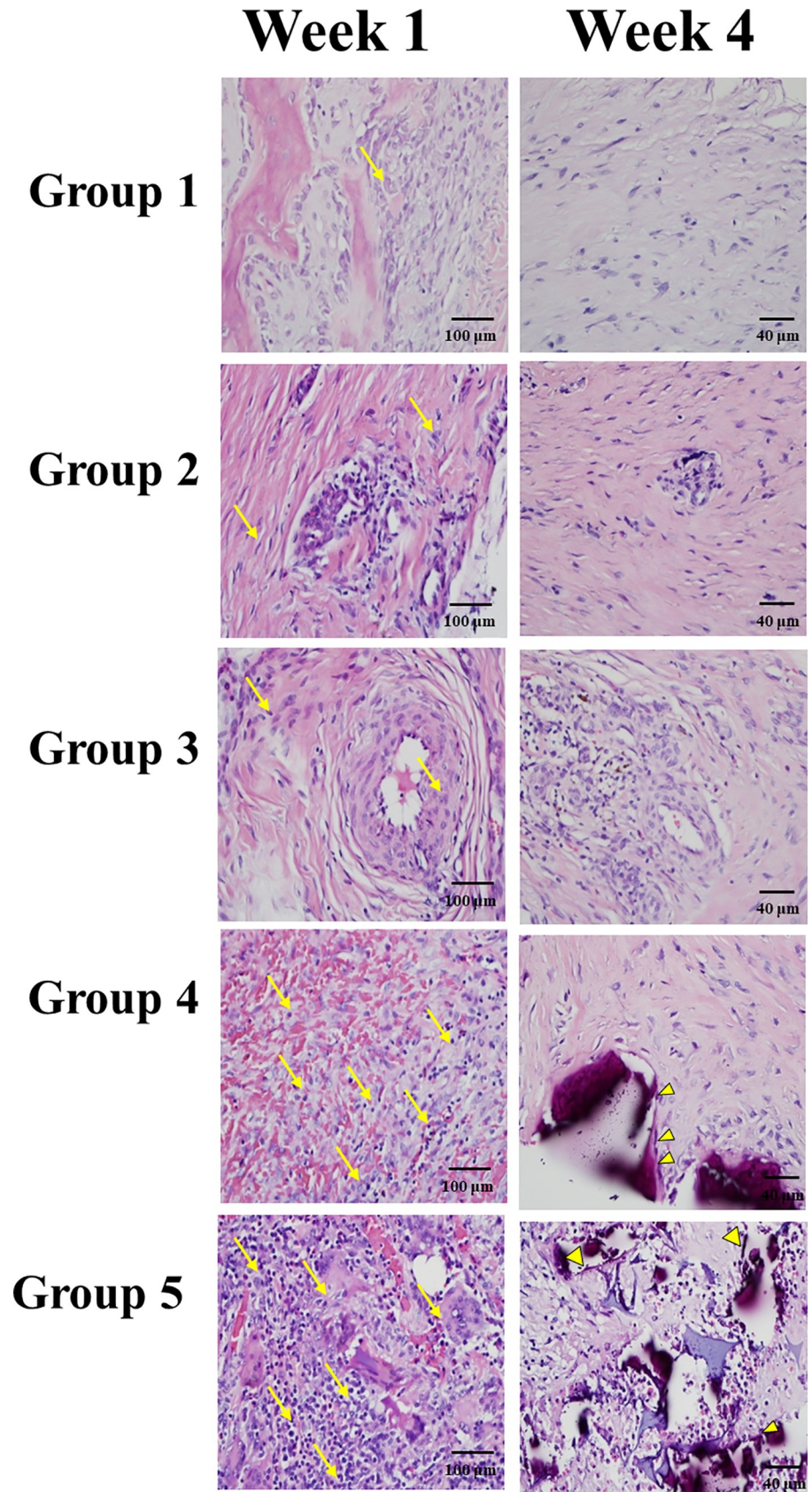
Fig 11. *In vivo* **Hematoxylin and eosin staining.** A greater number of cells were stained with H&E in groups 4 and 5 compared to groups 1–3 in the first week (yellow arrow). Osteoid formation was confirmed histologically in the hematoxylin and eosin-stained defect of group 4 and 5 at 4 weeks postoperatively (yellow arrowhead). Staining was observed in all groups in 400× magnification.

https://doi.org/10.1371/journal.pone.0215499.g011

Immunohistochemistry of osteogenic related markers

We conducted IHC analysis to evaluate OC,BSP-II and Col-I osteogenic related markers (Figs 14–16). IHC of OC, BSP-II and Col-I were highly expressed in group 4 and 5 than the other three groups through all culture period and suggested that more osteogenesis in group 4 and 5 in week 4 (Figs 14–16, arrows). IHC of Col-I was only poor expressed in group I but high expressed in group 2 and 3 (Fig 16.arrow heads) due to the scaffolds, hemostatic gelatin sponge, were highly composed of Col-I [36].

Discussion

Allografts may provide the same osteoconductive conduits for bony fusion as traditional autografts and may have comparable biomechanical properties [5, 6]. Although depleted of osteo-progenitor cells like MSCs, the fusion rate still reaches 73% to 100% in instrumented spinal fusion [7–16], making allografts a clinically feasible alternative for fusion. Cells, scaffolds, and factors are the triad of regenerative engineering, and the lack of one of these three graft properties made us wonder about the role of seeded cells in bone regeneration.

A number of studies examining the combination of MSCs and 3-D scaffolds in bone regeneration have reported promising outcomes in animal critical size bone defects [38–43]. These studies aimed to achieve the final result of bone repair by using different kinds of scaffolds [44], sources of MSCs [45] or loaded factors [46–48], but very few studies have focused on the role of the seeded cells.

Kuznetsova et al. [49] used allogenic transplantation of mice MSCs loaded on fabricated 3-D scaffolds made from poly (D, L)-lactic acid and hydroxyapatite in the calvarial defect. They divided the mice into two experimental groups: GFP (+) mice MSCs transplanted into GFP (-) mice and GFP(-) mice MSCs transplanted into GFP(+)mice; the scaffold without cells was used as the control. Fluorescence imaging and histology revealed only allogeneic cells on the scaffold after 6 weeks and 12 weeks, and newly formed bone-like tissue from seeded cells was detected by 12 weeks. The presence of vessels was confirmed by CD31 immunohistochemical staining, which indicated the possibility of vessel formation from seeded MSCs.

However, there were four major drawbacks of their study. First, the use of Hoechst stain in fluorescence imaging to indicate seeded or host cells is not reasonable because the GFP harvest of cells may decay after transplantation for 6 weeks or 12 weeks; cells with GFP may also stain with blue color, providing misleading results about the origin of cells. Second, the surface view of fluorescence imaging cannot represent the actual cell interactions during bone regeneration inside the 3-D scaffold. Third, the creation of only one defect in each mouse cannot eliminate individual variations. Fourth, bone formation was supposed to be similar in both experimental groups. The authors explained that GFP itself may be immunogenic in immunocompetent mice; however, GFP was present in both groups.

To the best of the authors' knowledge, the present study is the first to compare the distribution and proportion of seeded cells and host cells by tracking two fluorescent cells in the same scaffold in a pig critical-sized calvarial defect model.

To eliminate individual variations in the animal study, we used a critical-sized calvarial defect in pigs instead of rats due to the limited size of rats. As an animal model, we chose the domestic pig because its bone regeneration rates correlate well with those found in humans
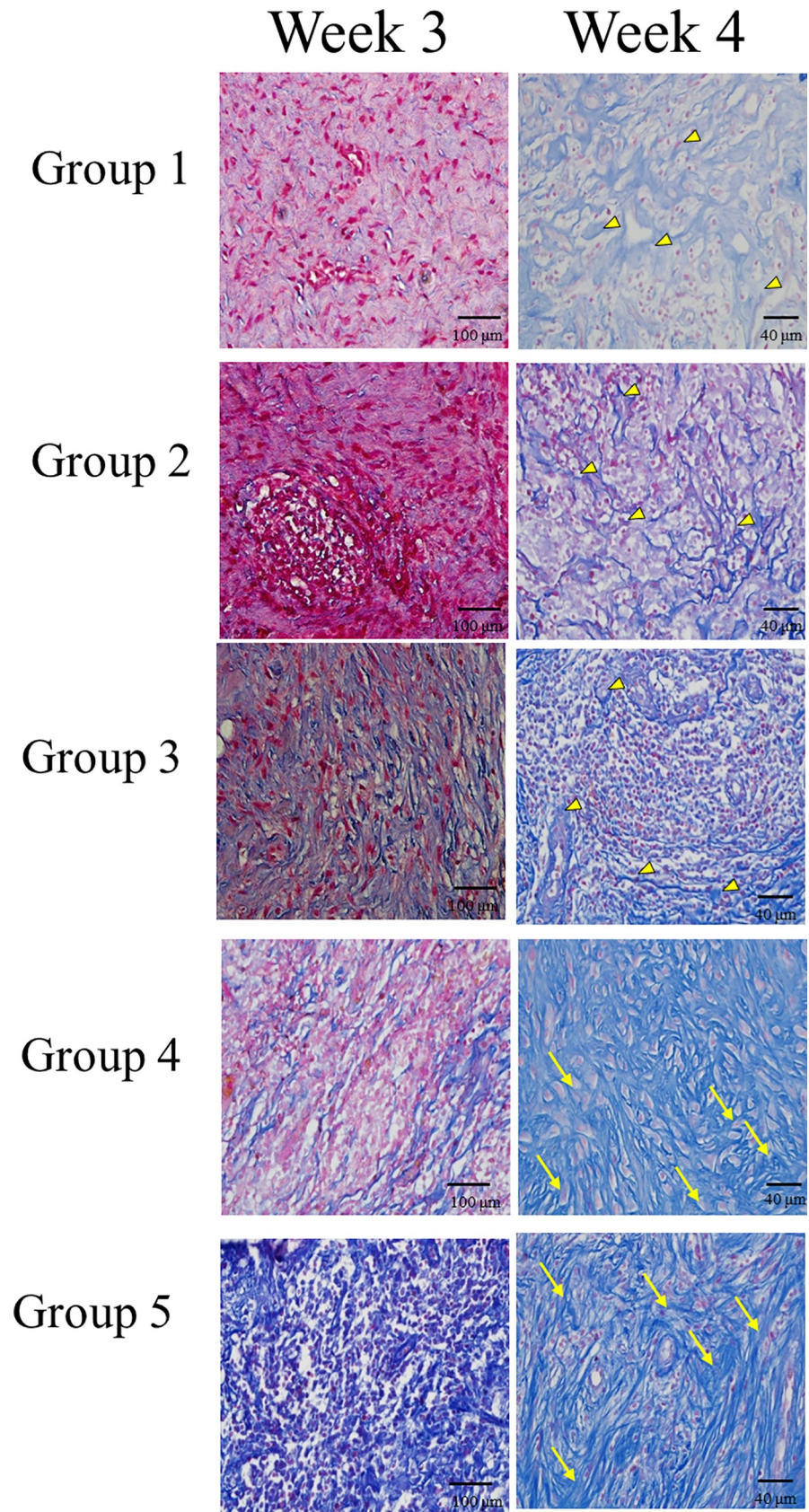
Fig 12. *In vivo* Masson's trichrome staining. Blue-colored osteoid-like tissue was only found in groups 4 and 5 after the third week. In the 4th week, in groups 4 and 5, thick dense fibrous connective tissue with differentiated osteoblast-like cells (yellow arrow) was noted but only a large amount of undifferentiated cells (yellow arrowhead) without obvious blue-colored osteoid-like tissue in groups 1, 2, and 3. Staining was observed in all groups in 400× magnification.

https://doi.org/10.1371/journal.pone.0215499.g012

(pigs 1.2–1.5 mm per day, humans 1.0–1.5 mm per day) [34]. Numerous experiments have been conducted to analyze bone formation with various scaffolds and factors in critical-sized calvarial defect pigs [50–52] because of the uniform, flat and surgically feasible calvarial bone. In general, a defect size with a diameter of at least 6mm is thought to be a reasonable critical-sized calvarial defect, and we also used an empty group (group 1) as a control.

The CAG hybrid promoter-driven EGFP-MSCs derived from the transgenic pigs used in this study have been proved to exhibit homogeneous surface epitopes and possess classic trilineage differentiation potential into osteogenic, adipogenic, and chondrogenic lineages, with robust EGFP expression maintained in all differentiated progeny. These cells have the major advantage of greater sustained EGFP expression in stem cells and in all their differentiated progeny [19] compared to GFP expression in transgenic pigs under the control of housekeeping regulatory sequences [53,54].Increased expression of green fluorescence was observed from day 3 to day 28 after culture into scaffolds (Figs 4 and 6)

The transgenic Ds-Red pigs were produced by using pronuclear microinjection, and the transgene comprised a CMV enhancer/chicken-beta actin promoter and DsRed monomeric cDNA [33]. DsRed is a red fluorescent protein that was originally discovered in corals of the class Anthozoa. DsRed is expressed ubiquitously, with red fluorescence detected in the brain, eye, tongue, heart, lung, liver, pancreas, spleen, stomach, small intestine, large intestine, kidney, testis, and muscle, as confirmed by histology and western blot analyses. Red fluorescence tracking was previously applied in transplantation of neurons from Ds-Red transgenic pigs into a Parkinson's disease rat model [55]. In this *in vivo* experiment, precise evaluation and analysis could be achieved due to the abundant expression of the two fluorescent proteins in all differentiated progeny.

The hemostatic gelatin sponge, Spongostan, is prepared from purified type A pork skin, and its biosafety in clinical applications, especially to control bleeding during surgery, has long been proved [56, 57]. *In vivo* studies have shown good biocompatibility of Spongostan™ without any immune response during bone formation [36]. The main reasons that we chose this scaffold are its biocompatibility and biodegradation with MSCs and absence of autofluorescence [36].

Our *in vivo* fluorescence analysis (Figs 9 and 10) showed that the green fluorescence in the scaffold loaded with seeded cells in groups 4 and 5 was significantly higher than that in the other groups from week 1 to week 4, which means that the seeded cells did play an important role in the osteogenic differentiation process. EGFP-pMSCs were highest in group 5 in the 4th week, which means that the higher load of seeded cells was sustained until the 4th week. DsRed expression (Fig 10) was highest in Group 4 in the 1st week, indicating that recruitment [58, 59] of host cells was facilitated in the lower density-seeded scaffold than the empty scaffold or higher density-seeded scaffold. DsRed expression decreased from the 1st week to 4th week in group 4 but increased in group 5, which means that more EGFP-pMSCs can recruit more host cells in the following period and that enough available space and higher cell loading benefit tissue regeneration. The higher expression of EGFP and DsRed fluorescence in groups 4 and 5 were compatible with the histological results, which indicated more obvious deposition of osteoids in groups 4 and 5 in week 4. The immunohistochemical results for CD68 in week 4 also showed obvious osteogenesis in groups 4 and 5.
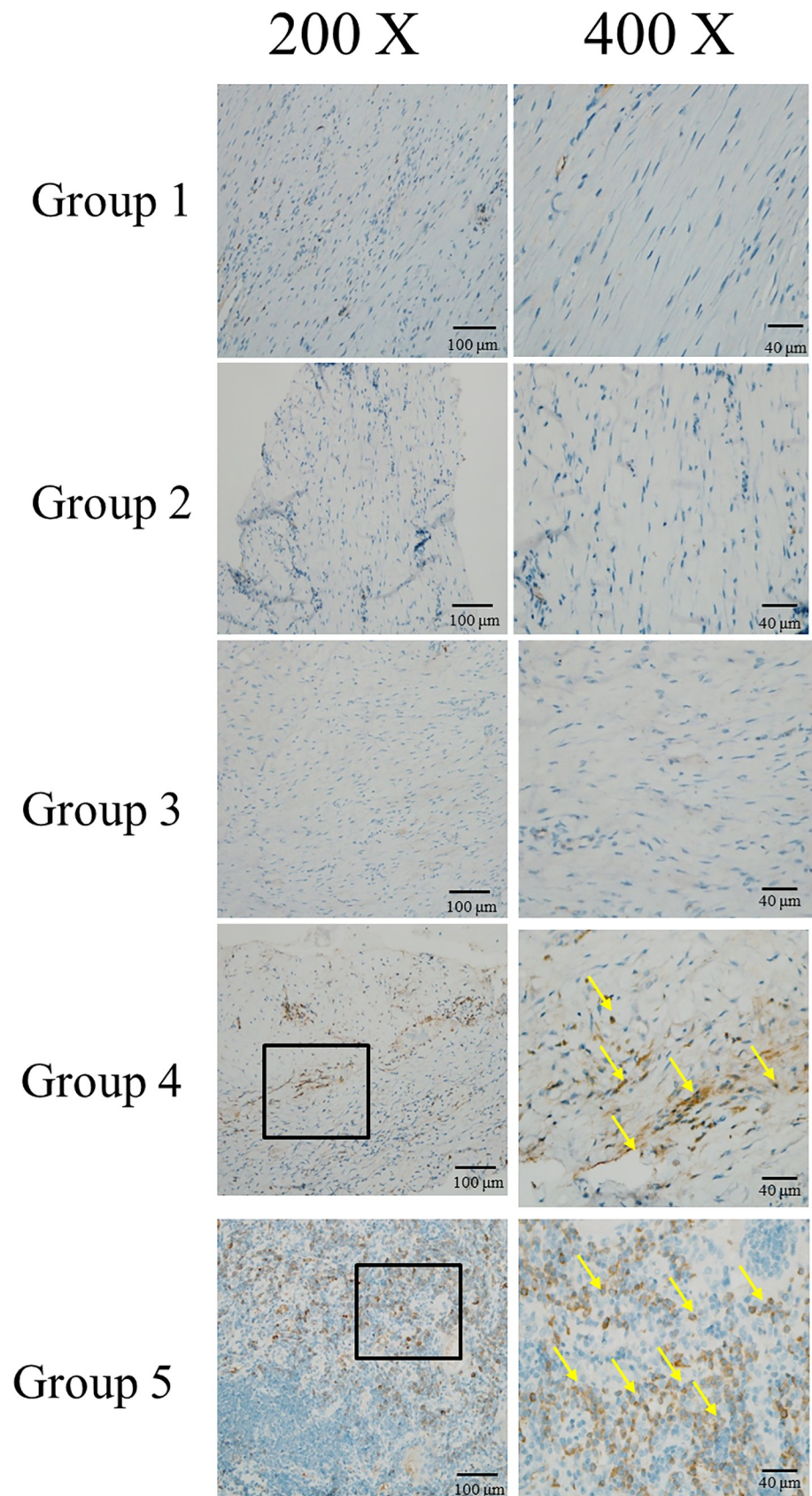
Fig 13. Immunohistochemistry of CD 68. The macrophage marker were stained with anti-CD68 antibody and marked with yellow arrow in group 4 and 5 in week 4. The increasing arrows, CD 68, in group 5 than group 4 suggested that more neovascularization and thus more osteogenesis in group 5 than group 4.

Fig 14. Immunohistochemistry of OC. IHC of OC was highly expressed in group 4 and 5 (yellow arrows) than the other three groups in week 4 and suggested that more osteogenesis in seeded cells group than empty cells group.

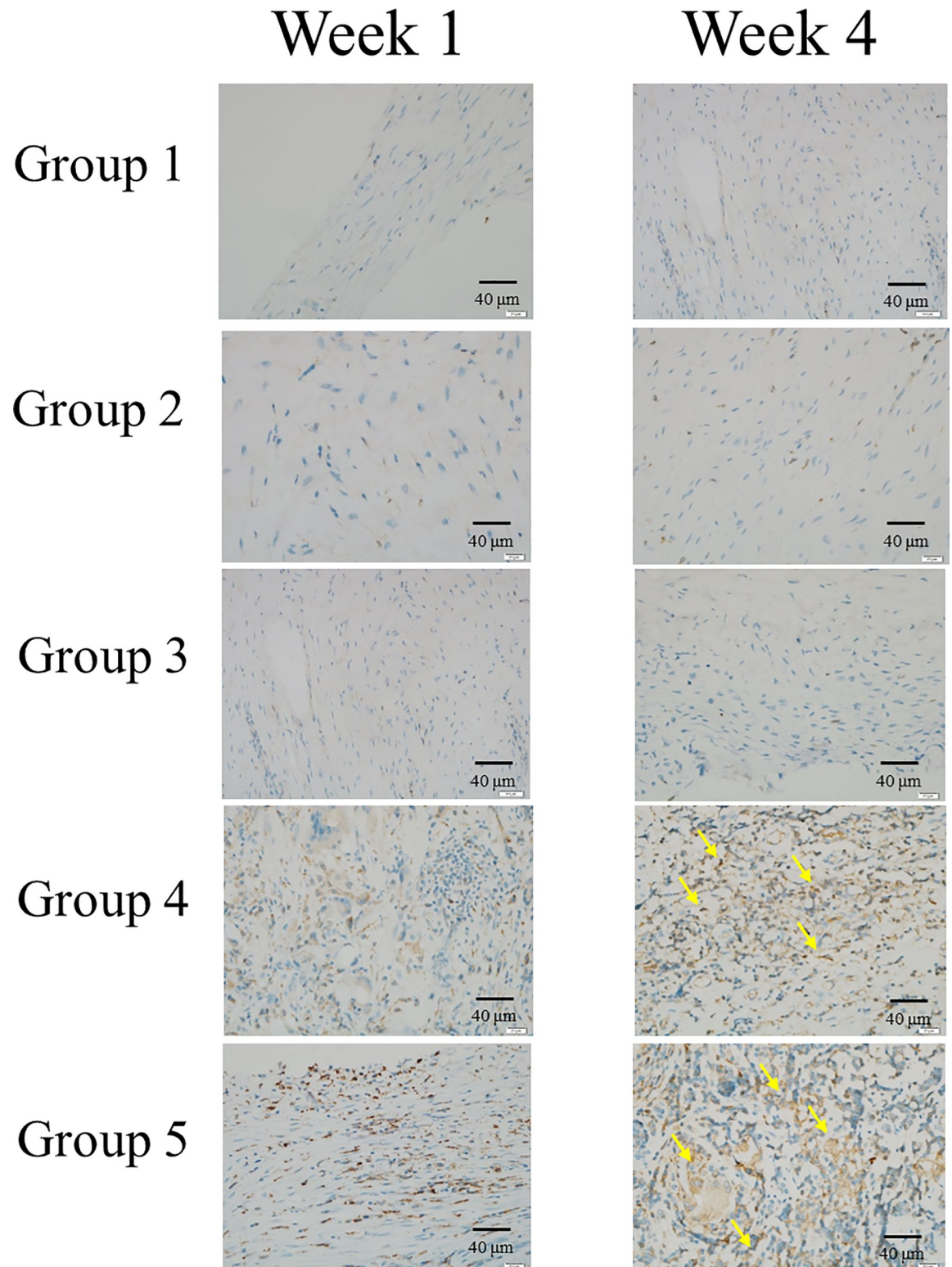https://doi.org/10.1371/journal.pone.0215499.g014
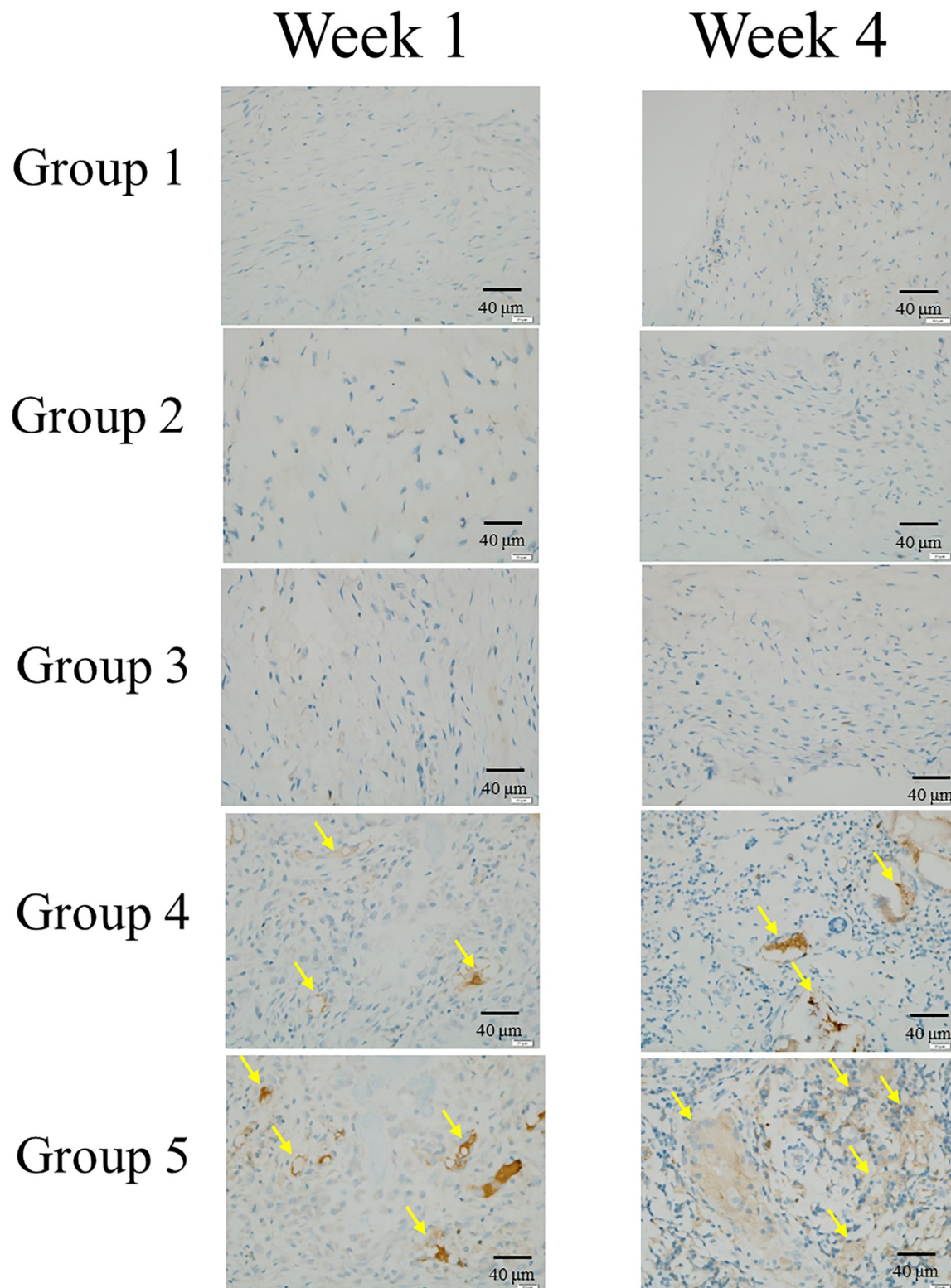
Fig 15. Immunohistochemistry of BSP-II. IHC of BSP-II was highly expressed in group 4 and 5 (yellow arrows) than the other three groups in week 1 and 4 and more expressed in group 5 than 4 which indicated that more osteogenesis in scaffolds with more seeded cells.

Week 1   Week 4

Fig 16. Immunohistochemistry of Col-I. IHC of Col-I was only poorly expressed in group I but highly expressed in groups 2 and 3 (arrow heads) due to the scaffolds, hemostatic gelatin sponge, were highly composed of Col-I.

https://doi.org/10.1371/journal.pone.0215499.g016

Our *in vivo* results demonstrated that the seeded MSCs promoted host cell migration, which contributed to the higher number of host cells in the transplanted scaffolds. In add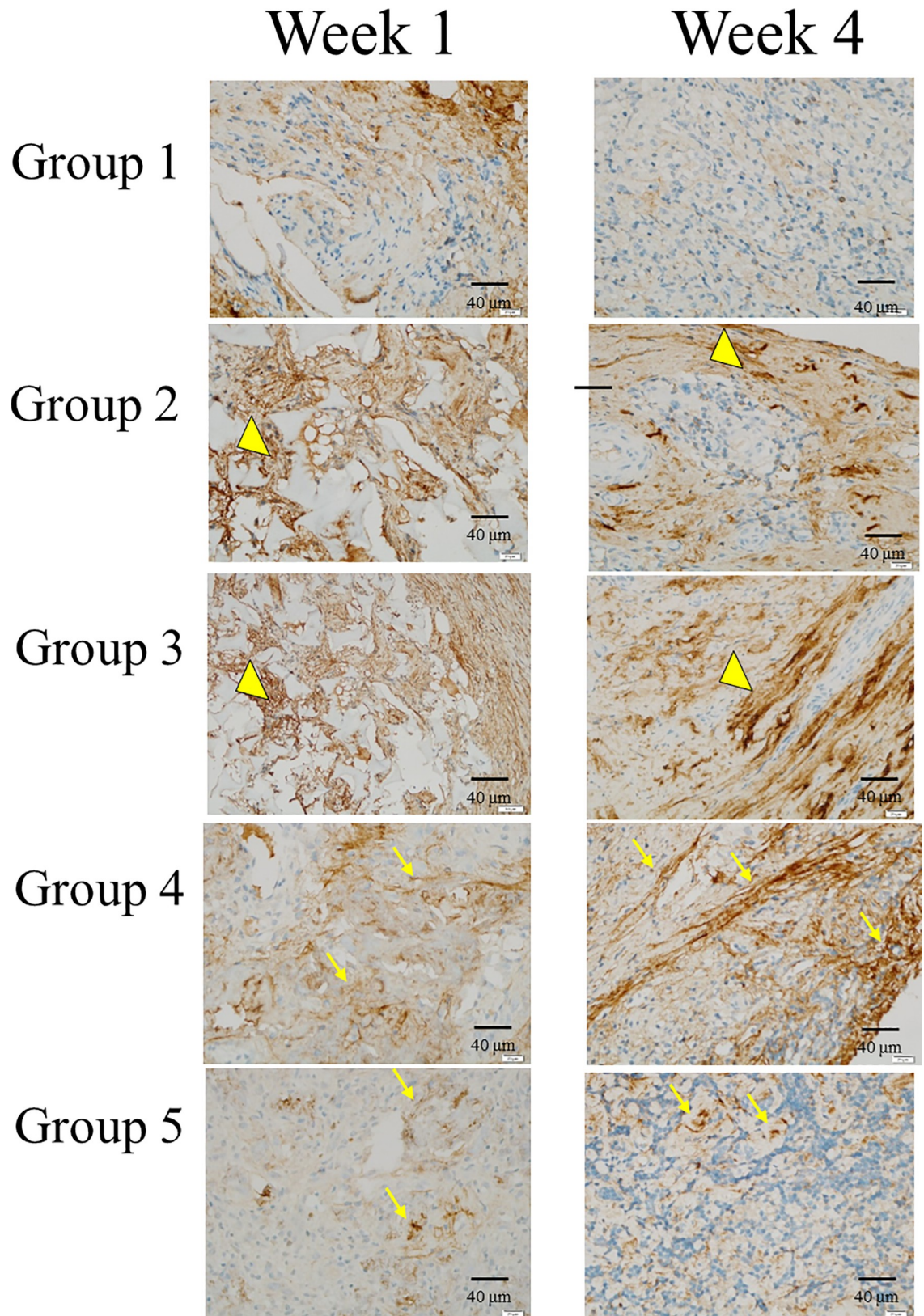ition, according to the histological staining, we found that the percentage of osteoid formation in the scaffolds transplanted with seeded MSCs was significantly higher than that in the control group, which means that not only the transplanted seeded cells but also the recruited host cells contributed to the entire process. Stem cells application such as human dental pulp stem cells (DPSCs) [60,61] reaches a breakthrough advancement in bone tissue engineering. DPSCs are derived from ectomesenchymal cells with the participation of neural crest-cell migration during organogenesis [60], can differentiate into osteoblasts, adipose cells, neurons, and smooth muscle regulated by different surrounding enviroment. Dental pulp stem cells have been sucssessfully used in human bone tissue engineering [61,62] and give rise to a 3D structure resembling a woven fibrous bone after 40 days of culture[63]. The data is similar with our finding that final bone formation was from not only the committed cells but also surrounding environmental change by proved angiogenesis[63]. The limitation of the study including short term data and fluorescence decay after stem cells differentiated into osteoblasts. In summary, we found that more seeded cells recruit more host cells and that both cell types participate in osteogenesis. Recruitment of host cells was facilitated in the lower density-seeded scaffold than the empty scaffold or higher density-seeded scaffold in the first week but sustained recruitment of host cells was achieved in higher density-seeded scaffold and result in more obvious deposition of osteoids. Scaffolds without seeded cells may therefore not be effective in bone transplantation based on this *in vivo* study.

Supporting information

S1 File. CD68 and IHC stain.
(ZIP)

S2 File. H&E stain data.
(ZIP)

S3 File. Masson's trichrome.
(ZIP)

S4 File. GFP result of all specimens.
(XLSX)

S5 File. RGB result of all specimens.
(XLSX)

Acknowledgments

Author Contributions

Conceptualization: Chia-Jung Wu.

Data curation: Ming-Kai Hsieh, Xuan-Chun Su, Tsung-Ting Tsai.

Formal analysis: Xuan-Chun Su, Yi-Chen Chen, Tsung-Ting Tsai.

Investigation: Chia-Jung Wu, Xuan-Chun Su, Tsung-Ting Tsai.

Methodology: Chi-Chien Niu, Shinn-Chih Wu.

Project administration: Ming-Kai Hsieh, Chi-Chien Niu.

Resources: Chia-Jung Wu, Chi-Chien Niu.

Software: Yi-Chen Chen.

Supervision: Po-Liang Lai, Shinn-Chih Wu.

Validation: Yi-Chen Chen, Po-Liang Lai.

Visualization: Ming-Kai Hsieh, Po-Liang Lai.

Writing – original draft: Ming-Kai Hsieh.

Writing – review & editing: Po-Liang Lai, Shinn-Chih Wu.

References

1. Bhumiratana S, Vunjak-Novakovic G. Concise review: personalized human bone grafts for reconstructing head and face. Stem Cells Transl Med. 2012; 1: 64–69. https://doi.org/10.5966/sctm.2011-0020 PMID: 23197642

2. Bauer TW, Muschler GF. Bone graft materials. An overview of the basic science. Clin Orthop Relat Res. 2000; 371: 10–27.

3. Kuznetsova D, Timashev P, Bagratashvili VN, Zagaynova EV. Scaffold- and cell system-based bone grafts in tissue engineering (review). Sovrem Tehnologii Med. 2014; 6: 201–211.

4. Chan BP, Leong KW. Scaffolding in tissue engineering: general approaches and tissue-specific considerations. Eur Spine J. 2008; 17: 467–479. https://doi.org/10.1007/s00586-008-0745-3 PMID: 19005702

5. Ryu SI, Lim JT, Kim S-M, Paterno J, Kim DH. Comparison of the biomechanical stability of dense cancellous allograft with tricortical iliac autograft and fibular allograft for cervical interbody fusion. Eur Spine J. 2006; 15: 1339–1345. https://doi.org/10.1007/s00586-005-0047-y PMID: 16429289

6. Godzik J, Ravindra VM, Ray WZ, Schmidt MH, Bisson EF, Dailey AT. Comparison of structural allograft and traditional autograft technique in occipitocervical fusion: radiological and clinical outcomes from a single institution. J Neurosurg Spine. 2015; 23: 144–152. https://doi.org/10.3171/2014.12.SPINE14535 PMID: 25955801

7. Knapp DR, Jones ET, Blanco JS, Flynn JC, Price CT. Allograft bone in spinal fusion for adolescent idiopathic scoliosis. J Spinal Disord Tech. 2005; 18: S73–S76. PMID: 15699809

8. Jones KC, Andrish J, Kuivila T, Gurd A. Radiographic outcomes using freeze-dried cancellous allograft bone for posterior spinal fusion in pediatric idiopathic scoliosis. J Pediatr Orthop. 2002; 22: 285–289. PMID: 11961440

9. Cabraja M, Kroppenstedt S. Bone grafting and substitutes in spine surgery. J Neurosurg Sci. 2012; 56: 87–95. PMID: 22617171

10. Rihn JA, Kirkpatrick K, Albert TJ. Graft options in posterolateral and posterior interbody lumbar fusion. Spine. 2010; 35: 1629–1639. https://doi.org/10.1097/BRS.0b013e3181d25803 PMID: 20628336

11. Andersen T, Christensen FB, Niedermann B, Helmig P, Hoy K, Hansen ES, et al. Impact of instrumentation in lumbar spinal fusion in elderly patients: 71 patients followed for 2–7 years. Acta Orthop. 2009; 80: 445–450. https://doi.org/10.3109/17453670903170505 PMID: 19626471

12. Ploumis A, Albert TJ, Brown Z, Mehbod AA, Transfeldt EE. Healos graft carrier with bone marrow aspirate instead of allograft as adjunct to local autograft for posterolateral fusion in degenerative lumbar scoliosis: a minimum 2-year follow-up study. J Neurosurg Spine. 2010; 13: 211–215. https://doi.org/10.3171/2010.3.SPINE09603 PMID: 20672956

13. Arnold PM, Robbins S, Paullus W, Faust S, Holt R, McGuire R. Clinical outcomes of lumbar degenerative disc disease treated with posterior lumbar interbody fusion allograft spacer: a prospective, multicenter trial with 2-year follow-up. Am J Orthop (Belle Mead NJ). 2009; 38: E115–E122.

14. Slosar PJ, Josey R, Reynolds J. Accelerating lumbar fusions by combining rhBMP-2 with allograft bone: a prospective analysis of interbody fusion rates and clinical outcomes. Spine J. 2007; 7: 301–307. https://doi.org/10.1016/j.spinee.2006.10.015 PMID: 17482113

15. Faundez AA, Schwender JD, Safriel Y, Gilbert TJ, Mehbod AA, Denis F, et al. Clinical and radiological outcome of anterior-posterior fusion versus transforaminal lumbar interbody fusion for symptomatic disc degeneration: a retrospective comparative study of 133 patients. Eur Spine J. 2009; 18: 203–211. https://doi.org/10.1007/s00586-008-0845-0 PMID: 19125304

16. Buser Z, Brodke DS, Youssef JA, Rometsch E, Park JB, Yoon ST, et al. Allograft versus demineralized bone matrix in instrumented and noninstrumented lumbar fusion: a systematic review. Global Spine J. 2018; 8: 396–412. https://doi.org/10.1177/2192568217735342 PMID: 29977726

17. Ohyama M, Okano H. Promise of human induced pluripotent stem cells in skin regeneration and investigation. J Invest Dermatol. 2014; 134: 605–609. https://doi.org/10.1038/jid.2013.376 PMID: 24132166

18. Michel J, Penna M, Kochen J, Cheung H. Recent advances in hydroxyapatite scaffolds containing mesenchymal stem cells. Stem Cells Int. 2015; 2015: 1–13.

19. Hsiao FS, Lian WS, Lin SP, Lin CJ, Lin YS, Cheng EC, et al. Toward an ideal animal model to trace donor cell fates after stem cell therapy: production of stably labeled multipotent mesenchymal stem cells from bone marrow of transgenic pigs harboring enhanced green fluorescence protein gene. J Anim Sci. 2011; 89: 3460–3472. https://doi.org/10.2527/jas.2011-3889 PMID: 21705633

20. Arpornmaeklong P, Brown SE, Wang Z, Krebsbach PH. Phenotypic characterization, osteoblastic differentiation, and bone regeneration capacity of human embryonic stem cell-derived mesenchymal stem cells. Stem Cells Dev. 2009; 18: 955–968. https://doi.org/10.1089/scd.2008.0310 PMID: 19327009

21. Lee JY, Choo JE, Choi YS, Shim IK, Lee SJ, Seol YJ, et al. Effect of immobilized cell-binding peptides on chitosan membranes for osteoblastic differentiation of mesenchymal stem cells. Biotechnol Appl Biochem. 2009; 52: 69–77. https://doi.org/10.1042/BA20070169 PMID: 18307409

22. Amini AR, Laurencin CT, Nukavarapu SP. Bone tissue engineering: recent advances and challenges. Crit Rev Biomed Eng. 2012; 40: 363–408. PMID: 23339648

23. Mauney JR, Volloch V, Kaplan DL. Role of adult mesenchymal stem cells in bone tissue engineering applications: current status and future prospects. Tissue Eng. 2005; 11: 787–802. https://doi.org/10.1089/ten.2005.11.787 PMID: 15998219

24. Tasso R, Ulivi V, Reverberi D, Io Sicco C, Descalzi F, Cancedda R. *In vivo* implanted bone marrow-derived mesenchymal stem cells trigger a cascade of cellular events leading to the formation of an ectopic bone regenerative niche. Stem Cells Dev. 2013; 22: 3178–3191. https://doi.org/10.1089/scd.2013.0313 PMID: 23924051

25. Gamblin AL, Brennan MA, Renaud A, Yagita H, Lezot F, Heymann D, et al. Bone tissue formation with human mesenchymal stem cells and biphasic calcium phosphate ceramics: the local implication of osteoclasts and macrophages. Biomaterials. 2014; 35: 9660–9667. https://doi.org/10.1016/j.biomaterials.2014.08.018 PMID: 25176068

26. Kulkarni M, Greiser U, O'Brien T, Pandit A. Liposomal gene delivery mediated by tissue-engineered scaffolds. Trends Biotechnol. 2010; 28: 28–36. https://doi.org/10.1016/j.tibtech.2009.10.003 PMID: 19896228

27. Lei Y, Segura T. DNA delivery from matrix metalloproteinase degradable poly(ethylene glycol) hydrogels to mouse cloned mesenchymal stem cells. Biomaterials. 2009; 30: 254–265. https://doi.org/10.1016/j.biomaterials.2008.09.027 PMID: 18838159

28. Sun XD, Jeng L, Bolliet C, Olsen BR, Spector M. Non-viral endostatin plasmid transfection of mesenchymal stem cells via collagen scaffolds. Biomaterials. 2009; 30: 1222–1231. https://doi.org/10.1016/j.biomaterials.2008.10.020 PMID: 19059640

29. Mulder G, Tallis AJ, Marshall VT, Mozingo D, Phillips L, Pierce GF, et al. Treatment of nonhealing diabetic foot ulcers with a platelet-derived growth factor gene-activated matrix (GAM501): results of a phase 1/2 trial. Wound Repair Regen. 2009; 17: 772–779. https://doi.org/10.1111/j.1524-475X.2009.00541.x PMID: 19821960

30. Sapet C, Formosa C, Sicard F, Bertosio E, Zelphati O, Laurent N. 3D-fection: cell transfection within 3D scaffolds and hydrogels. Ther Deliv. 2013; 4: 673–685. https://doi.org/10.4155/tde.13.36 PMID: 23738666

31. Villa MM, Wang L, Rowe DW, Wei M. Effects of cell-attachment and extracellular matrix on bone formation *in vivo* in collagen-hydroxyapatite scaffolds. PLoS One. 2014; 9: e109568. https://doi.org/10.1371/journal.pone.0109568 PMID: 25329879

32. Jensen J, Tvedesoe C, Rolfing JH, Foldager CB, Lysdahl H, Kraft DC, et al. Dental pulp-derived stromal cells exhibit a higher osteogenic potency than bone marrow-derived stromal cells *in vitro* and in a porcine critical-size bone defect model. SICOT J. 2016; 2: 16. https://doi.org/10.1051/sicotj/2016004 PMID: 27163105

33. Chou C-J, Peng S-Y, Wu M-H, Yang C-C, Lin Y-S, Cheng WT-K, et al. Generation and characterization of a transgenic pig carrying a DsRed-monomer reporter gene. PLoS One. 2014; 9: e106864. https://doi.org/10.1371/journal.pone.0106864 PMID: 25187950

34. Schlegel KA, Lang FJ, Donath K, Kulow JT, Wiltfang J. The monocortical critical size bone defect as an alternative experimental model in testing bone substitute materials. Oral Surg Oral Med Oral Pathol Oral Radiol Endod. 2006; 102: 7–13. https://doi.org/10.1016/j.tripleo.2005.09.011 PMID: 16831666

35. Wehrhan F, Amann K, Molenberg A, Lutz R, Neukam FW, Schlegel KA. PEG matrix enables cell-mediated local BMP-2 gene delivery and increased bone formation in a porcine critical size defect model of craniofacial bone regeneration. Clin Oral Implants Res. 2012; 23: 805–813. https://doi.org/10.1111/j.1600-0501.2011.02223.x PMID: 22151397

36. Kuo Z-K, Lai P-L, Toh EK-W, Weng C-H, Tseng H-W, Chang P-Z, et al. Osteogenic differentiation of preosteoblasts on a hemostatic gelatin sponge. Sci Rep. 2016; 6: 32884. https://doi.org/10.1038/srep32884 PMID: 27616161

37. Hsieh M-K, Wu C-J, Chen C-C, Tsai T-T, Niu C-C, Wu S-C, et al. BMP-2 gene transfection of bone marrow stromal cells to induce osteoblastic differentiation in a rat calvarial defect model. Mater Sci Eng C. 2018; 91: 806–816.

38. Mangano C, de Rosa A, Desiderio V, d'Aquino R, Piattelli A, de Francesco F, et al. The osteoblastic differentiation of dental pulp stem cells and bone formation on different titanium surface textures. Biomaterials. 2010; 31: 3543–3551. https://doi.org/10.1016/j.biomaterials.2010.01.056 PMID: 20122719

39. Ito K, Yamada Y, Nakamura S, Ueda M. Osteogenic potential of effective bone engineering using dental pulp stem cells, bone marrow stem cells, and periosteal cells for osseointegration of dental implants. Int J Oral Maxillofac Implants. 2011; 26: 947–954. PMID: 22010075

40. Qin Y, Guan J, Zhang C. Mesenchymal stem cells: mechanisms and role in bone regeneration. Postgrad Med J. 2014; 90: 643–647. https://doi.org/10.1136/postgradmedj-2013-132387 PMID: 25335795

41. Patel D, Shah J, Srivastava A. Therapeutic potential of mesenchymal stem cells in regenerative medicine. Stem Cells Int 2013; 49: 21–28.

42. Koob S, Torio-Padron N, Stark GB, Hannig C, Stankovic Z, Finkenzeller G. Bone formation and neovascularization mediated by mesenchymal stem cells and endothelial cells in critical-sized calvarial defects. Tissue Eng Part A. 2011; 17: 311–321. https://doi.org/10.1089/ten.TEA.2010.0338 PMID: 20799886

43. Nassif L, Sabban M. Mesenchymal stem cells in combination with scaffolds for bone tissue engineering. Materials (Basel). 2011; 4: 1793–1804.

44. Kwon DY, Kwon JS, Park SH, Park JH, Jang SH, Yin XY, et al. A computer-designed scaffold for bone regeneration within cranial defect using human dental pulp stem cells. Sci Rep. 2015; 5: 12721. https://doi.org/10.1038/srep12721 PMID: 26234712

45. Kargozar S, Mozafari M, Hashemian SJ, Milan P, Hamzehlou S, Soleimani M, et al. Osteogenic potential of stem cells-seeded bioactive nanocomposite scaffolds: a comparative study between human mesenchymal stem cells derived from bone, umbilical cord Wharton's jelly, and adipose tissue. J Biomed Mater Res B Appl Biomater. 2018; 106: 61–72. https://doi.org/10.1002/jbm.b.33814 PMID: 27862947

46. Raftery RM, Mencia-Castano I, Sperger S, Chen G, Cavanagh B, Feichtinger GA, et al. Delivery of the improved BMP-2-Advanced plasmid DNA within a gene-activated scaffold accelerates mesenchymal stem cell osteogenesis and critical size defect repair. J Control Release. 2018; 283: 20–31. https://doi.org/10.1016/j.jconrel.2018.05.022 PMID: 29782946

47. Guo J, Wu G. The signaling and functions of heterodimeric bone morphogenetic proteins. Cytokine Growth Factor Rev. 2012; 23: 61–67. https://doi.org/10.1016/j.cytogfr.2012.02.001 PMID: 22421241

48. Annamalai RT, Turner PA, Carson WF, Levi B, Kunkel S, Stegemann JP. Harnessing macrophage-mediated degradation of gelatin microspheres for spatiotemporal control of BMP2 release. Biomaterials. 2018; 161: 216–227. https://doi.org/10.1016/j.biomaterials.2018.01.040 PMID: 29421557

49. Kuznetsova D, Prodanets N, Rodimova S, Antonov E, Meleshina A, Timashev P, et al. Study of the involvement of allogeneic MSCs in bone formation using the model of transgenic mice. Cell Adh Migr. 2016; 11: 233–244. https://doi.org/10.1080/19336918.2016.1202386 PMID: 27314915

50. Park J, Lutz R, Felszeghy E, Wiltfang J, Nkenke E, Neukam FW, et al. The effect on bone regeneration of a liposomal vector to deliver BMP-2 gene to bone grafts in peri-implant bone defects. Biomaterials. 2007; 28: 2772–2782. https://doi.org/10.1016/j.biomaterials.2007.02.009 PMID: 17339051

51. Stockmann P, Park J, von Wilmowsky C, Nkenke E, Felszeghy E, Dehner JF, et al. Guided bone regeneration in pig calvarial bone defects using autologous mesenchymal stem/progenitor cells—a comparison of different tissue sources. J Craniomaxillofac Surg. 2012; 40: 310–320. https://doi.org/10.1016/j.jcms.2011.05.004 PMID: 21723141

52. Bornstein MM, Heynen G, Bosshardt DD, Buser D. Effect of two bioabsorbable barrier membranes on bone regeneration of standardized defects in calvarial bone: a comparative histomorphometric study in pigs. J Periodontol. 2009; 80: 1289–1299. https://doi.org/10.1902/jop.2009.090075 PMID: 19656029

53. Nowak-Imialek M, Kues WA, Petersen B, Lucas-Hahn A, Herrmann D, Haridoss S, et al. Oct4-enhanced green fluorescent protein transgenic pigs: a new large animal model for reprogramming studies. Stem Cells Dev. 2011; 20: 1563–1575. https://doi.org/10.1089/scd.2010.0399 PMID: 21126163

54. Yong HY, Hao Y, Lai L, Li R, Murphy CN, Rieke A, et al. Production of a transgenic piglet by a sperm injection technique in which no chemical or physical treatments were used for oocytes or sperm. Mol Reprod Dev. 2006; 73: 595–599. https://doi.org/10.1002/mrd.20477 PMID: 16489622

55. Chiu CH, Li IH, Weng SJ, Huang YS, Wu SC, Chou TK, et al. PET imaging of serotonin transporters with 4-[(18)F]-ADAM in a parkinsonian rat model with porcine neural xenografts. Cell Transplant. 2016; 25: 301–311. https://doi.org/10.3727/096368915X688236 PMID: 25994923

56. Seo JP, Tsuzuki N, Haneda S, Yamada K, Furuoka H, Tabata Y, et al. Osteoinductivity of gelatin/beta-tricalcium phosphate sponges loaded with different concentrations of mesenchymal stem cells and bone morphogenetic protein-2 in an equine bone defect model. Vet Res Commun. 2014; 38: 73–80. https://doi.org/10.1007/s11259-013-9587-5 PMID: 24442646

57. Amjadian S, Seyedjafari E, Zeynali B, Shabani I. The synergistic effect of nano-hydroxyapatite and dexamethasone in the fibrous delivery system of gelatin and poly(l-lactide) on the osteogenesis of mesenchymal stem cells. Int J Pharm. 2016; 507: 1–11. https://doi.org/10.1016/j.ijpharm.2016.04.032 PMID: 27107902

58. Lin W, Xu L, Zwingenberger S, Gibon E, Goodman SB, Li G. Mesenchymal stem cells homing to improve bone healing. J Orthop Translat. 2017; 9: 19–27. https://doi.org/10.1016/j.jot.2017.03.002 PMID: 29662796

59. Xu L, Huang S, Hou Y, Liu Y, Ni M, Meng F, et al. Sox11-modified mesenchymal stem cells (MSCs) accelerate bone fracture healing: sox11 regulates differentiation and migration of MSCs. FASEB J. 2015; 29: 1143–1152. https://doi.org/10.1096/fj.14-254169 PMID: 25466891

60. d'Aquino R, Tirino V, Desiderio V, Studer M, De Angelis GC, Laino L,et al. Human neural crest-derived postnatal cells exhibit remarkable embryonic attributes either in vitro or in vivo. Eur Cell Mater. 2011 Mar 22; 21:304–16. PMID: 21432784

61. Spina A, Montella R, Liccardo D, De Rosa A, Laino L, Mitsiadis TA,et al. NZ-GMP Approved Serum Improve hDPSC Osteogenic Commitment and Increase Angiogenic Factor Expression. Front Physiol. 2016 Aug 19; 7:354. https://doi.org/10.3389/fphys.2016.00354 PMID: 27594842

62. Pisciotta A, Bertoni L, Riccio M, Mapelli J, Bigiani A, La Noce M, et al. Use of a 3D Floating Sphere Culture System to Maintain the Neural Crest-Related Properties of Human Dental Pulp Stem Cells. Front Physiol. 2018 May 28; 9:547. https://doi.org/10.3389/fphys.2018.00547 PMID: 29892229

63. Paino F, La Noce M, Giuliani A, De Rosa A, Mazzoni S, Laino L,et al. Human DPSCs fabricate vascularized woven bone tissue: a new tool in bone tissue engineering.Clin Sci (Lond). 2017 Apr 25; 131 (8):699–713.